Nitric Oxide Recombination to Double Mutants of Myoglobin: Role of Ligand Diffusion in a Fluctuating Heme Pocket[†,Δ]

M. L. Carlson,[‡] Rebecca Regan,[‡] Ron Elber,[§] Haiying Li,[∥] G. N. Phillips, Jr.,[⊥] J. S. Olson,[⊥] and Q. H. Gibson*[,‡]

Department of Biochemistry, Molecular and Cell Biology, Cornell University, Ithaca, New York 14853, Department of Chemistry, University of Illinois at Chicago, Chicago, Illinois 60680, The Fritz Haber Research Center, The Hebrew University, Givat Ram, Jerusalem 91904, Israel, and Department of Biochemistry and Cell Biology and W. M. Keck Center for Computational Biology, Rice University, Houston, Texas 77251-1892

Received March 23, 1994; Revised Manuscript Received June 17, 1994[⊗]

ABSTRACT: Picosecond recombination of nitric oxide to the double mutants of myoglobin, His64Gly·Val68Ala and His64Gly·Val68Ile, at E7 and E11, has been studied experimentally and by computation. It is shown that distal residues have a profound effect on NO recombination. Recombination in the mutants may be explained in terms of fluctuating free volume and structure of the heme pocket. The double mutants provide insight into the effects of free volume and steric hindrance on rates of ligand rebinding following photolysis. Water molecules of the first solvation shell replace surface residues deleted by mutation and can block apparent holes in the protein structure. Thus, water molecules extend the time required for ligands to escape significantly to a nanosecond time scale, which is much longer than would be expected for an open heme pocket. Both nearly exponential (G64A68) and markedly nonexponential (native and G64I68) kinetics are observed, a result at variance with expectation from the model of Petrich et al. [Petrich, J. W., Lambry, J. C., Kuczera, K., Karplus, M., Poyart, C., & Martin, J. L. (1991) *Biochemistry 30,* 3975–3987], which attributes nonexponential kinetics to proximal effects.

The recombination of nitric oxide with heme iron in myoglobin following flash photolysis is particularly well suited for comparing molecular dynamics simulations with experiment because of three favorable experimental factors. These are the speed of the reaction which, with a half-time in tens of picoseconds (Cornelius et al., 1981; Jongeward et al., 1988; Petrich et al., 1988), is within the reach of molecular dynamics computation, the ability to make specific alterations in structure by site-directed mutagenesis (Springer & Sligar, 1987; Egeberg et al., 1990), and the availability of high-resolution X-ray crystallographic data giving soundly based starting points for computation (Phillips et al., 1990; Carver et al., 1992).The first investigations using these tools (Gibson et al., 1992) showed that mutations at position B10 in the distal heme pocket alter the rate of NO recombination markedly; substituting Phe for Leu (the residue in the native protein) made it faster, and substituting Ala and Val for Leu slowed it down. This result led naturally to the simple supposition that the rate of geminate recombination depends on the volume available to ligand molecules in the heme pocket. The larger the free volume, the less likely ligand molecules are to be near enough to the iron atom to recombine with it, so the rate of geminate rebinding should be determined by the space available in the distal pocket.

Molecular dynamics simulations and experimental results with other mutant myoglobins have suggested that this simple picture requires elaboration (Carver et al., 1990; Gibson et al., 1992). The heme pocket is not a static structure but should rather be thought of as a transient and mobile volume defined by the side chains of the residues in the helices on the distal side of the heme group. As the volume accessible to ligand molecules is not constant and does not always include the iron atom, the probability of ligand recombination in a given time interval may vary widely for different atomic coordinates of the same protein. The rate of the overall recombination reaction, observed experimentally, is the sum of the individual atomic recombination processes and will be exponential if the lifetime of the fluctuating pocket structures is short as compared with the rate of the recombination reaction or nonexponential if individual pocket structures persist for long periods when compared with the time required for recombination. Computation showed structures long-lived in relation to the time scales of recombination, in agreement with the experimental observation of a nonexponential time course of NO rebinding (Jongeward et al., 1986; Petrich et al., 1988; Gibson et al., 1992; Walda et al., 1994). Our present experimental and computational data do not allow a distinction to be drawn between phenomenological models of diffusive protein motion (Agmon & Rabinovich, 1992) and models with rapid transitions between relatively long-lived protein states (Austin et al., 1975; Ansari et al., 1986).

To reduce steric restraints adjacent to the ligand binding site, Egeberg et al. (1990) prepared the double mutant His64Gly·Val68Ala (G64A68). They expected that the volume of the distal pocket would be greatly increased, facilitating movement of ligands relative to the iron atom. Before picosecond experiments with NO were performed, the rate of geminate recombination was expected to be lower than in native myoglobin. Experiment, however, showed that the

[†] M.L.C., R.R., and Q.H.G. were supported by U.S. Public Health Service Grant GM14276 (to Q.H.G.), R.E. and H.L. were supported by U.S. Public Health Service Grant GM41905 and by the Department of Energy, G.N.P. was supported by U.S. Public Health Service Grant AR 40252 and Grant C1142 from the Robert A. Welch Foundation and the W. M. Keck Foundation, and J.S.O. was supported by U.S. Public Health Service Grants GM35649 and HL47020 and Grant C612 from the Robert A. Welch Foundation and the W. M. Keck Foundation.

[Δ] Coordinates have been deposited in the Brookhaven Protein Data Bank (Entry 1MLU).

* To whom correspondence should be addressed at the Department of Biochemistry.

[‡] Cornell University.

[§] The Hebrew University.

[∥] University of Illinois.

[⊥] Rice University.

[⊗] Abstract published in *Advance ACS Abstracts,* August 1, 1994.

0006-2960/94/0433-10597$04.50/0

Table 1: Summary of Crystallographic Statistics[a]

resolution	1.90 Å	RMS_{bond}	0.024 Å
completeness	87%	RMS_{angles}	2.7°
R_{merge}	3.7%	$RMS_{dihedral}$	21.7°
R_{cryst}	14.5%	$RMS_{improper}$	5.1°

[a] R_{merge} is the agreement based on intensities of 24 240 comparisons of data from scans in two orientations. R_{cryst} is the final crystallographic R-factor after refinement. RMS deviations are from the output of XPLOR.

rate of geminate recombination was greater than in native myoglobin, a result at first attributed to collapse of the heme pocket reducing its volume. Another mutant, G64I68, with less free volume in the heme pocket, instead of recombining with NO faster than G64A68, actually rebound much more slowly, a result analogous to the low rate of geminate NO recombination observed for the single mutant V68I (Carver et al., 1990; Ikeda-Saito et al., 1993).

The results with these mutants illustrate an additional problem. His64 is near the surface of the protein, and it has been proposed and widely accepted that movement of its side chain may function as a gate, controlling access and escape of the ligand (Case & Karplus, 1979; Case & Kottalam, 1988; Johnson et al., 1989). It was expected, therefore, that replacement of the imidazole side chain with glycine would be associated with rapid escape of ligand from the pocket, an effect which did not occur (Carver et al., 1990).

In earlier work, mutants with substitutions for Val68 (E11) have given mixed results; V68F reacted rapidly, as expected, but V68I reacted more slowly (Carver et al., 1990). Further, the implicit assumption that the origin of these effects is to be found in the distal heme pocket is at variance with an alternative molecular model (Petrich et al., 1991) which relates the rate of ligand rebinding to the distance of the iron atom from the plane of the porphyrin. This provides a time-dependent barrier for ligand binding that leads to nonexponential recombination, a scheme fundamentally different from the transient-volume model discussed above. It focuses on the protein structure on the proximal side of the heme, while the transient-volume model focuses on its distal side. The unexpected results with the double mutants and the conflict in interpretation call for the further investigation of the double mutants presented here.

MATERIALS AND METHODS

(A) Experiment. Plasmids containing the double mutations were constructed and given to us by Karen D. Egeberg, Barry A. Springer, and Steven G. Sligar from the University of Illinois, Champaign-Urbana (Egeberg et al., 1990). The genes were expressed constitutively in *Escherichia coli* TB-1 cells using the 100-L fermentation facility at Rice University, and the mutant proteins were purified as described by Springer et al. (1989).

The structure of the double mutant G64A68 was determined by refinement starting from the wild-type CO derivative published previously by Quillin et al. (1993), PDB entry 2MGK. Crystals were grown as described in Phillips et al. (1990). Data were collected on a Siemens X-100A area detector and processed using XDS (Kabsch, 1988). R_{sym} was 3.3%. XPLOR version 3.0 (Brunger & Karplus, 1988) was used for the refinement with the PROLSQ parameter set. Statistical results of the data collection and refinement are given in Table 1. Coordinates have been deposited at the Brookhaven Data Bank.

Picosecond kinetic data were collected using a YAG mode-locked laser giving 35-ps pulses, frequency doubled to 532 nm. The pulses were split and part of the used pulses to perform photolysis; the remainder were passed through a Raman tube filled with hydrogen at 15 atm to give observation pulses at 436 nm.

(B) Computation. The calculations were performed using the molecular dynamics program MOIL (Elber et al., 1994). The cutoff distance for the nonbonded interactions was 9 Å, and the 1–4 scaling factors for van der Waals and electrostatic interactions were 8 and 2, respectively. The time step was 2 fs, and all the bonds were "shaked" (Ryckaert et al., 1977). The X-ray structures of the native and the G64A68 mutant were used to initiate the simulations. The starting structure used for G64I68 is discussed in the Results section. Simulations were run for three proteins: H64V68 (native), G64A68, and G64I68. All crystallographic water molecules (about 130 total), modeled by TIP3P (Jorgensen et al., 1983), were included in the simulation. The water molecules provide a partial solvation shell for the neighborhood of the heme. This shell is crucial in maintaining the normal heme structure and a reasonable conformation of the distal histidine, where present. For each of the proteins at least 10 trajectories 50 ps long were computed. In the trajectories 15 ps was used for equilibration and 35 ps was considered a production run.

The calculations used the locally enhanced sampling (LES) protocol as implemented in MOIL (Elber et al., 1994). In LES simulations a number of ligand copies (say 10) share the same protein trajectory. The multiple trajectories of the ligand copies provide significantly enhanced statistics as compared to the usual molecular dynamics runs that include only one copy of the ligand. The LES trajectories are based on a mean field approach in which the protein experiences the average force of all the ligands and must, therefore, be regarded as approximate. In a recent study LES trajectories were compared with trajectories of single ligand molecular dynamics and with a revised form of LES including binary collisions (Li et al., 1993). The relative rates of ligand diffusion in the different mutants were well reproduced, although the ligand copies in the LES were more mobile than single ligands in the usual trajectories. The LES trajectories require less computation, and if relative rather than absolute rates of recombination are required, the LES protocol seems adequate. The computations reported here describe the relative rates of recombination in the native (genetically engineered version of the native protein) and the double mutants G64A68 and G64I68.

RESULTS

(A) Structure of the Mutant G64A68. Average structures of wild-type myoglobin and the double mutant have been compared by examining the results from X-ray crystallography. The structure of the CO-bound form of G64A68 has been determined to 1.9-Å resolution. No major rearrangements relative to the wild type result from the substitutions, but there are packing adjustments in the vicinity of the distal pocket. As a result of the removal of the C_γ methyl groups from the side chain of residue Val68 (E11), the pocket collapses slightly (Figure 1), with the C_z atom of Phe43 (CD1) and the C_β atom of Ala68 (E11) moving closer together (7.1 versus 7.8 Å in the native). The C_α of Gly64 (E7) also moves toward the ligand by about 1.0 Å, and the terminal methylene group of Ile107 (G8) rotates toward the ligand, reducing the total distance from the back of the pocket to the front from 11.4 to 9.6 Å. In place of the imidazole of the distal His64 (E7), a well-ordered water molecule is positioned to interact with polar ligands, as in the Gly64 (E7) single mutant (Quillin et al., 1993).

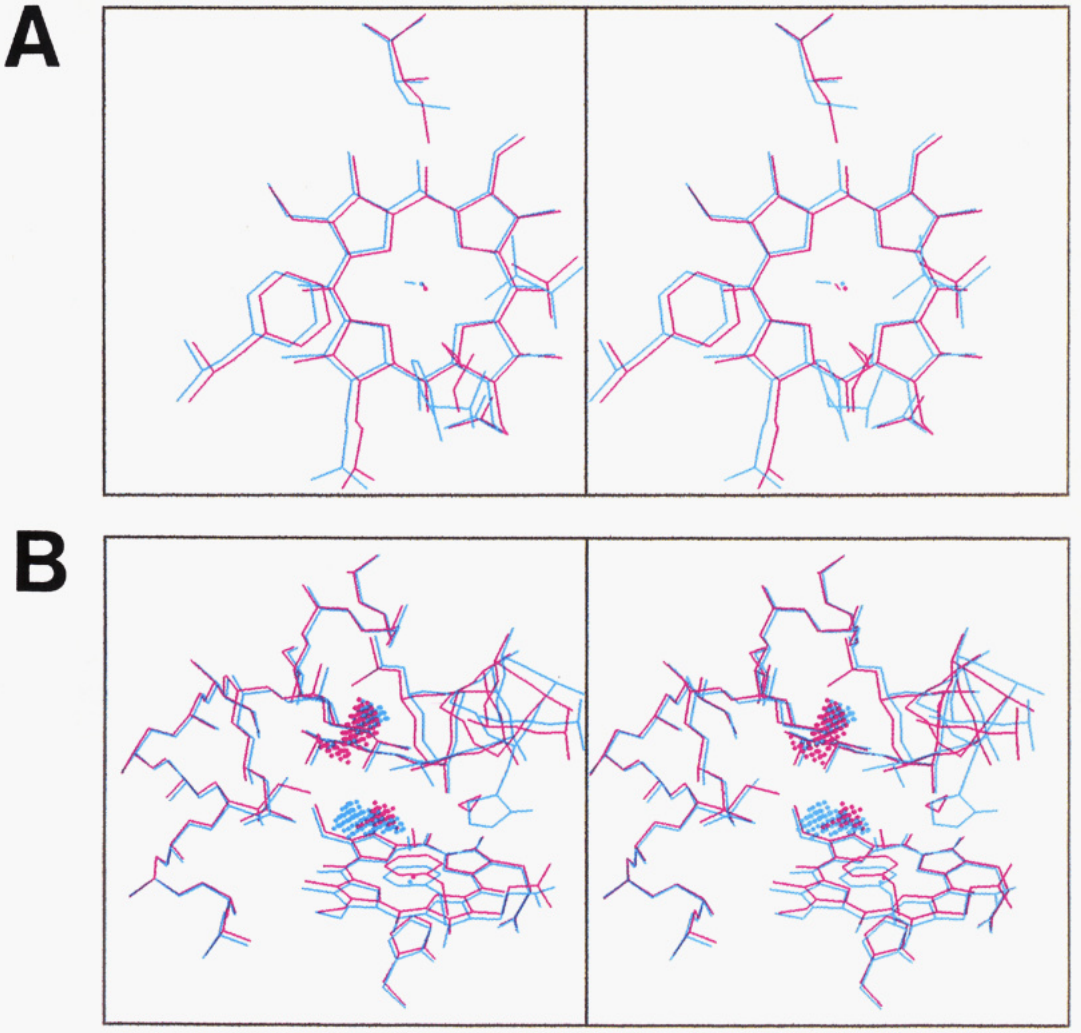

FIGURE 1: Panel A: Stereoview of the heme pocket in native (cyan) and in the double mutant G64A68 (red). The view is from above the distal side of the heme group, and only the immediately relevant residues are shown: for the wild-type (cyan) these are His64, Val68, Ile107, and Phe43. Note the inward movement of the residues in the mutant (red). Panel B: Spaces in the heme pocket region in native (cyan dots) and G64A68 (red dots). A dot is placed at each point on a search grid (0.3 Å) found to be 3.2 or more Å from any atom in the structure (excluding ligand atoms).

The coordinates from the crystal structures can also be used to examine the probe-accessible volumes on the distal side of the heme. While the X-ray structure does not reflect any local changes that may be associated with protein expansion following photolysis (Richard et al., 1992), it allows the free volume in the pocket to be visualized (Figure 1). The compensating compaction described above leads to similar volumes in G64A68 and native, but of different shapes. The effects of the mutations seen in the molecular dynamics simulations for these proteins cannot, therefore, be due to simple volume effects, but rather reflect the complex potential surface of the side-chain configurations.

(B) Picosecond Kinetics. The experimental results for NO recombination relevant to the computations are confined to data obtained during the first nanosecond or so after flash photolysis, and representative results are shown in Figure 2. In panel A data taken from earlier work show the effect of two single substitutions at position E11, each of a residue bulkier than the native valine (Carver et al., 1990). It is obvious that the effects of the two substitutions are opposite. In the time of observation much less NO recombines with V68I than with V68F.

Panel B of Figure 2 compares the two double mutants, G64A68 and G64I68, together with data for native sperm whale myoglobin (Gibson et al., 1992). As with the data of panel A, the effect of the substitutions is opposite to earlier expectation, with rapid and extensive recombination in G64A68 and slow and partial recombination in G64I68.

(C) Analysis of Molecular Dynamics Trajectories. The histograms of Figure 3 show the number of ligand molecules within 4 Å of the heme iron, counted at the end of each picosecond, cumulated for each run, and arranged in ascending order. This procedure does not give information about absolute rates of NO rebinding, but the totals for the various B10 mutants have been found to correlate well with the experimental rates (Gibson et al., 1992). This is true for the double mutants also, with the largest number of close approaches for G64A68, the least for G64I68 and native intermediate, which is the order in the experiment of in Figure 2.

The positive correlation with experiment encouraged examination of the trajectories in more detail and their description at the atomic level. The list of residues approached closely by ligands is illustrated in Figure 4 with the number of encounters shown by the height of the bars. It is obvious that, as often happens, if the ligands are confined to a single restricted space during a run, the list of residues is likely to be short, to vary little with time, and to define the residues limiting the space available to the ligands. Data for two separate runs with native myoglobin are presented, one with 23 approaches to the iron atom in 50 ps and one with 525

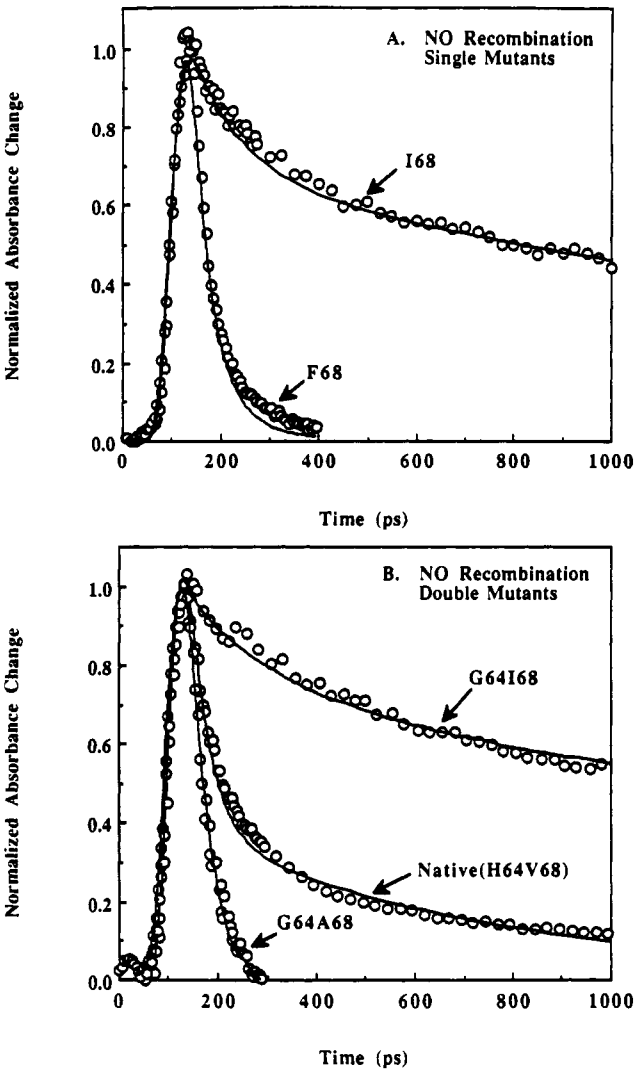

FIGURE 2: Time course of NO rebinding to native and mutant myoglobins following flash photolysis. The proteins were examined at pH 9 in 0.1 M borate buffer after equilibration with 5% NO gas in nitrogen. The concentration was ≈80 μM in heme in each case, the path length was 1 mm, and observation was at 436 nm at room temperature. The ordinate is the normalized change in absorbance at each time from the value before the flash. The abscissa began before the 35-ps flash and recording continued for 1.5 ns thereafter. Panel A reproduces data taken from Carver et al. (1990). Panel B shows data for the double mutants G64A68 and G64I68 and for native sperm whale myoglobin prepared by the same process but without mutation.

approaches in the same time. The differences are quantitative rather than qualitative. In the run with fewer approaches to the iron (23 collisions), there are more collisions with Leu29 and fewer with Phe43, His64, and Val68. The motion of the group of ligands has much the same azimuth relative to the heme plane in both runs, but the ligands are further from the iron in the direction perpendicular to the porphyrin plane in the run with 23 collisions with the iron.

The mutants differ appreciably from the native and from each other. The mutant G64I68 shows relatively fewer ligand approaches to Leu29 and Ile107 (the specific example in Figure 4 has none) and many encounters with water molecules. The mutant G64A68 has considerably more encounters with those two residues but still far fewer than is the case with wild type. In both double mutants, the ligand group moves toward the space normally occupied by the side chain of His64 and not toward Ile107, so the motion is opposite in azimuth to that in native myoglobin.

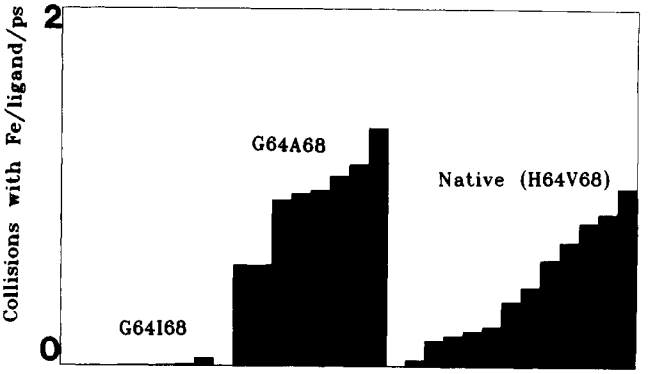

FIGURE 3: Average number of collisions per picosecond for multiple simulations of ligand rebinding to native sperm whale myoglobin and the mutants G64A68 and G64I68. Any ligand atom at a distance ≤4 Å from the iron atom was counted as a collision, and 10 ligand copies were used in each simulation. The average was calculated by summing the number of collisions at 1-ps intervals and dividing by the number of ligand copies and the total time of the simulation. In this calculation the maximum frequency of collision with the iron was 2 per ligand per picosecond (one for each ligand atom). Each column represents a 50-ps run started with a different initial atomic velocity distribution. The bars are arranged in ascending order of collision frequency with the smallest on the left and the largest on the right for each mutant.

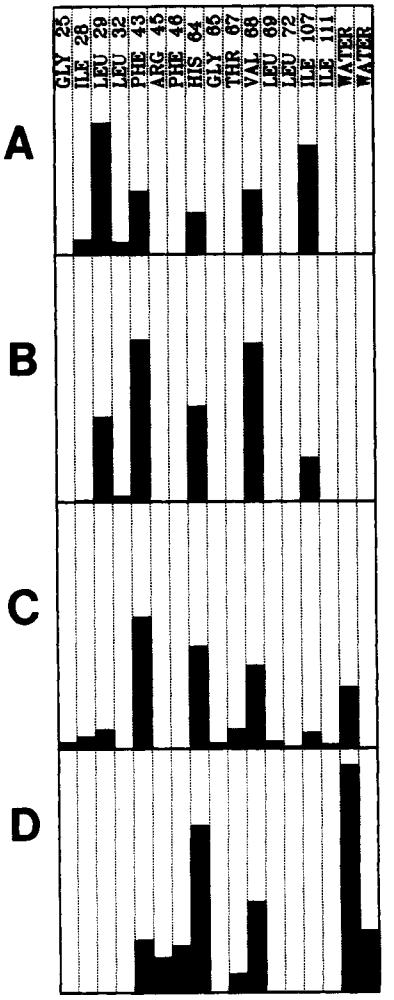

FIGURE 4: Number of close approaches (4 Å) of ligands to any atom of the residues indicated at the top of the figure. Data are presented for two LES simulations of native sperm whale myoglobin with different numbers of collisions with heme iron. Rows: A, 23 collisions; B, 525 collisions; C, G64A68; D, G64I68. Note that the ligands are far from the iron atom and are cut off from it by Ile68.

These results are presented semischematically in Figure 5, which compares wild-type myoglobin with the mutants. The

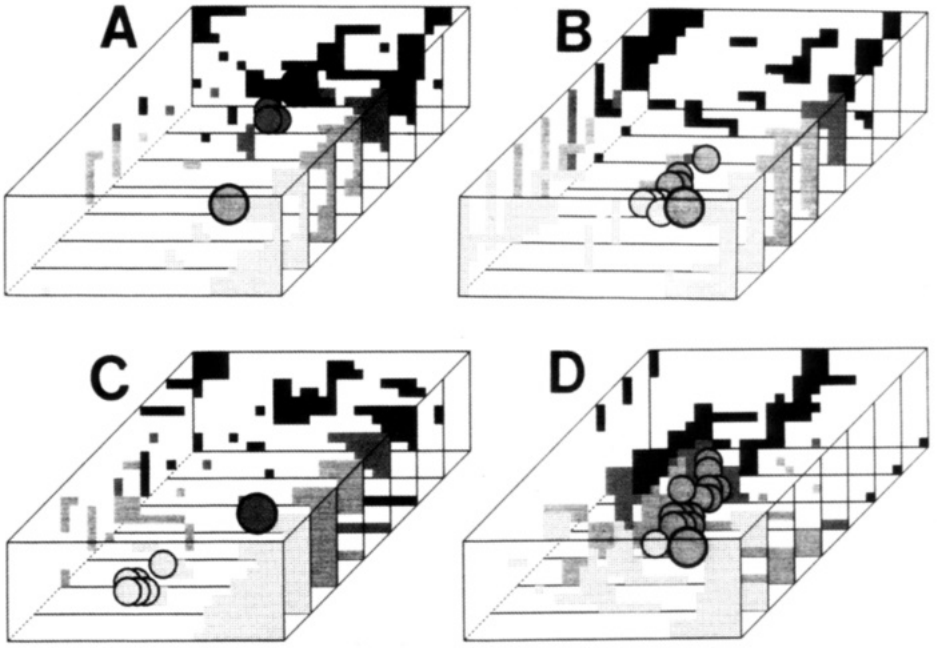

FIGURE 5: Schematic presentation of the positions of ligands and spaces in the neighborhood of the heme pocket at the end of 50-ps simulations. The heme forms the floor of the box, and the slices are separated by 1 Å. The iron atom is larger and has a heavy border; ligands are shaded to correspond with the shading of the slices in which they are found. Phe43 is to the left, Ile107 and Ile111 are toward the rear, Val68 is to the right, and Leu29 is along the top. Parts A and B are two runs with native sperm whale myoglobin, with small and large numbers of collisions, respectively. Part C is for G64I68 and part D for G64A68. Note that in part C the iron atom is far from the ligands and cut off from them.

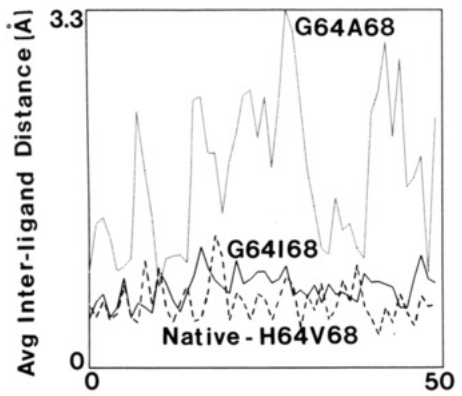

FIGURE 6: Mean distance between the centers of ligand copies during LES simulation runs. The ordinate is the sum of the distances between ligands 1 and 2–10, 2 and 3–10, ..., divided by the total number of distances (45) measured at each picosecond of simulation. Data are presented for G64I68 (continuous line), G64A68 (dotted line), and native myoglobin (dashed line). The ordinate is the mean distance in angstroms.

shaded areas show empty space in the heme pocket region divided into 1-Å slices, and the ligands (circles) have the same density as the slice to which they belong. The figures for the native are for simulations with low and high collision numbers. It is evident that in one case the ligand group is confined near the heme iron and in the other is both more remote and cut off from it. In G64I68 the ligands are remote from the iron and have moved in almost exactly the opposite direction to that taken in the native protein. It is clear that in this double mutant there is no path which would allow the return of the ligands to the iron.

Animations of the runs showed that the ligands form a looser group in G64A68 than in native or in G64I68 myoglobin. This is illustrated in Figure 6 where the mean distance between the centers of the ligands is plotted for one native run and for the two mutants. It is evident that the distance is similar, small, and varies little during the run for the native and G64I68 proteins.

The average distance of the ligands from the iron atom in G64A68 is much larger and more variable, a result reflecting the distribution of ligands between a space close to the iron and more remote spaces (Figure 7). In this figure, the height of each bar is proportional to the number of ligand molecules close to the iron at the end of each picosecond, and results are given for several runs with each myoglobin. The results for native have been reported (Gibson et al., 1992). They show large divergences between runs different only in the initial distribution of atomic velocities. Both mutants are more consistent in behavior between runs: in G64I68 there are very few ligand molecules close to the iron at any time. In G64A68 the number fluctuates randomly with an average of about five molecules within 4 Å.

An additional element in the computed behavior of the native and the double mutants is illustrated in Figure 8. The stereo pairs show the positions of the backbone atoms at intervals of 5 ps after the beginning of the computer runs. Although too many residues are shown to permit the resolution of atomic detail, it is obvious that the three pairs form a graded series with minimal movement in the native and maximal movement in G64A68. Replacement of the side chain of His64 by water molecules, while impeding the escape of ligand molecules from the heme pocket, does not substitute for the unyielding imidazole ring in defining the packing of the helices, and in the simulations, relatively large movements of the E-helix and of the heme occur during the runs.

Some of the results of computation are presented in Figure 9. The atoms of residues immediately around the iron atom on the distal side of the porphyrin plane are represented by spheres with van der Waals radii. In each case the view is through the heme group which is represented by a stick diagram.

In the upper row, two frames are shown for a LES run with native myoglobin in which the ligand group (white) shifted from a stable position remote from the iron (more than 4 Å) to another stable position nearer at hand. For the first half of the run (27-ps frame), the center of the ligand group is out

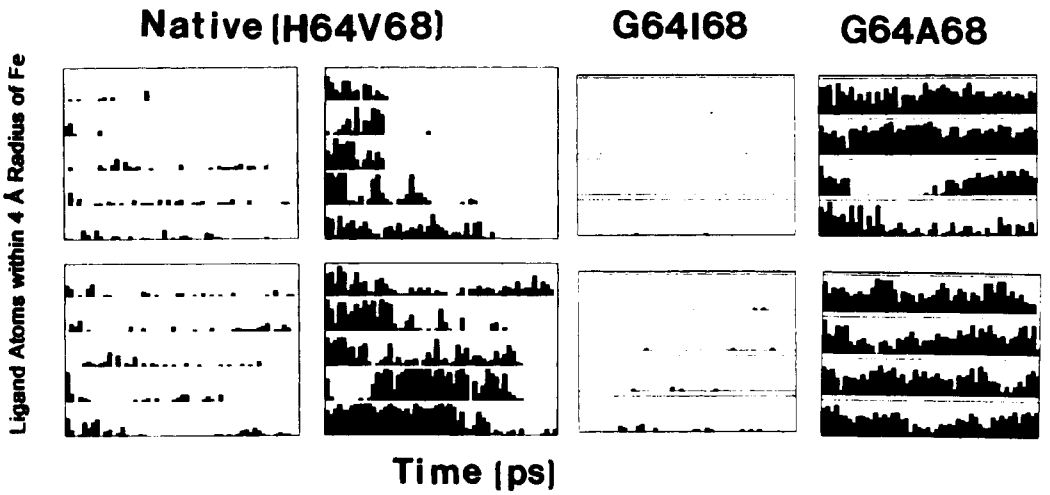

FIGURE 7: Location of ligand copies as a function of time in simulations of myoglobins. Each row represents an individual simulation starting with a different random distribution of initial atomic velocities. The time scale is 0–50 ps for the complete panels. Each filled bar represents the number of ligand copies within 4 Å of the iron atom at each picoseconds of simulation.

of line with the iron atom and is surrounded by the residues identified in the stick diagram (third panel in the row). In the earlier frame the distal histidine (E7, green) is directly in line with the iron atom and blocks ligands from approaching it. In the later frame (49 ps), the distal histidine and Val E11 have moved upward, and the ligand group is nearly in line with the iron which is now readily accessible. In the double mutant G64A68 (Figure 9, middle row) the mutated residues are shown in green. The ligands continue to be retained in the heme pocket because the substantial loss of residue bulk in the upper right-hand quadrant of the frame (E7 and E11) is made good by water molecules (blue) stabilized by interaction with the heme propionates and with each other. Complete escape of ligand from G64A68 to solvent does not occur readily, according to the results of nanosecond experiments with the CO derivative. While geminate recombination of CO in native MbCO, and in many mutants, accounts for some 5% of photodissociated CO, the proportion with G64A68 is some 10 times larger (Figure 10). The implication is that ligands which leave the vicinity of the iron do not escape from the protein at once but are retained for a period measured in tens of nanoseconds.

Since a crystal structure for G64I68 is not currently available, other structures were hybridized to create starting coordinates for the simulations. One started from coordinates generated from the structure for native myoglobin and its associated water molecules (PDB 2MGK), substituting Ile for Val68 in the orientation taken from the structure of Ile68·Fe(III) (M. L. Quillin and G. N. Phillips, Jr., unpublished results) and excising the side chain of His64. The structure of the mutant Gly64 (Quillin et al., 1993) was used to generate a second starting structure for G64I68. It has a water molecule deep within the pocket. It was converted to G64I68 by substitution of Ile for Val68 (E11) in the position taken from a more recent determination of the coordinates of the single mutant Ile68·CO (M. L. Quillin and G. N. Phillips, Jr., unpublished results). The behavior of the two structures during simulation was reassuringly similar. (Unless specified, all results emanate from the first structure.)

The lower row of frames in Figure 9 is for G64I68. As in the other frames, the mutated residues are shown in green, with the exception that the atom C_δ of Ile68 is shown in purple. The left-hand frame shows the positions of the atoms at the beginning of the run. The ligand cloud is directly in line with the iron, and C_δ is off center. In the later frame the ligands have moved away, and C_δ has moved upward, in part replacing the ligands, which cannot return to within 4 Å of the iron unless C_δ is displaced. As in G64A68, His64 (E7) is replaced by water molecules.

The results of simulations with the second starting structure also agree well with the data of Figure 2 and show the additional feature that the water molecule present in the heme pocket of G64, which was retained in the computer version of G64I68, regularly moved over the iron after the ligands had moved away. This water molecule appeared to be performing the same function as C_δ of Ile68 in the other group of simulations, blocking ligand access to the iron atom.

In a small number of runs with G64I68 a complete recombination model was used to simulate NO rebinding (Li et al., 1993). In most cases, the single ligand molecule moved into the space normally occupied by the side chain of His64. In a few cases the ligand started away from the iron in the opposite direction (i.e., toward Ile107), approached the water molecule in the pocket, returned toward the iron, and was recaptured by it early in the simulation.

DISCUSSION

Two important factors that influence the recombination rate have been identified by the combined use of mutants, simulations, kinetic experiments, and X-ray data. The first is the major role of steric hindrance in determining the recombination rate. It has been suggested that, depending on its orientation, the distal histidine may control access of ligand to the binding site. Although the distal histidine is usually associated with stabilizing interactions with oxygen, such as hydrogen bond formation, here, the kinematic effect is clearly the opposite. The second factor, demonstrated in the mutants, is the secondary barrier to ligand escape from the heme pocket formed by specific members of the solvation shell of water molecules around the protein. These molecules are well-defined [all the water molecules used in computation come from X-ray data either for the mutant itself or (G64I68) for its parent molecule] and in the G64A68 and G64I68 mutants are sufficient to retain the ligand molecules in the heme pocket for many picoseconds.

In earlier work, it was reported that the addition of a water shell with over 900 molecules had little effect on ligand recombination simulations with the B10 mutants (Gibson et al., 1992). The reason is that the simulation time is too short

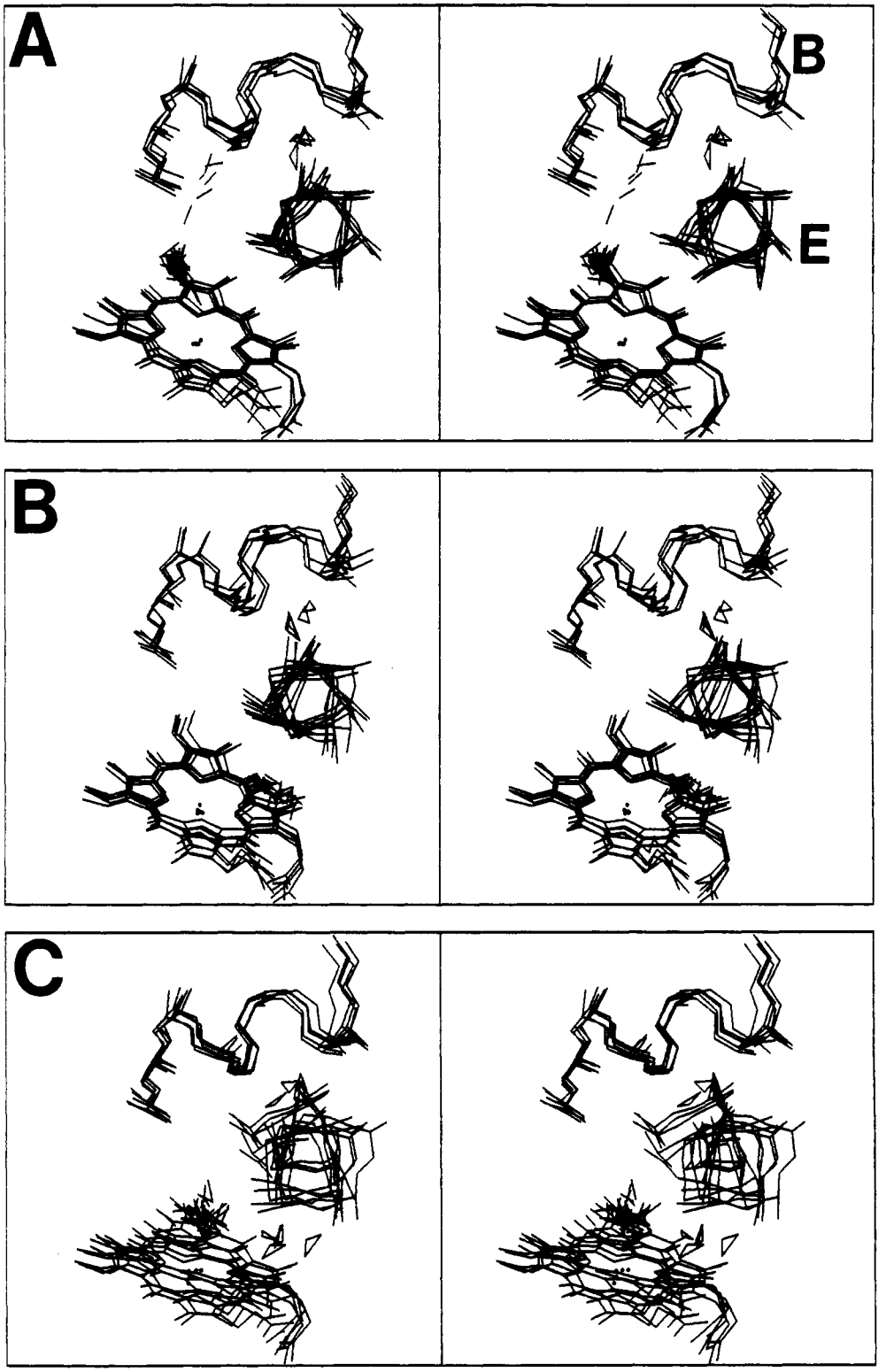

FIGURE 8: Stereo pairs showing corresponding parts of the native, G64I68, and G64A68 myoglobins looking along the axis of the E-helix. A fragment of the B-helix is in the upper part of each frame; the heme, some water molecules, and ligand copies are below. The positions of the atoms are shown at intervals of 5 ps during a 50-ps simulation. In the native protein the ligands are held in a compact group between the iron atom and the rear of the pocket. In G64I68 the group is less compact and is between the iron atom and the front of the pocket. In G64A68 the ligands are spread through a relatively large volume directly above the iron atom.

to allow long-range solvation forces to influence the calculated diffusion of the ligand significantly. Further, except in G64I68, the ligand motion in the subnanosecond time range is toward the center of the protein and so is unlikely to be influenced by external solvent.

On the other hand, when residues such as His64 that are in a direct contact with the external solvent molecules are modified, more significant effects of solvation may be expected and, indeed, are seen. In a vacuum simulation of the single G64 mutant, the ligand copies streamed out readily on a picosecond time scale (R. Elber, unpublished results). However, when water molecules were added in proper locations and numbers, the hole in the pocket created by the mutation was filled and the original structure remained intact. In earlier studies, comparing simulations with a complete solvation shell and a partial solvation shell, a small number of water molecules

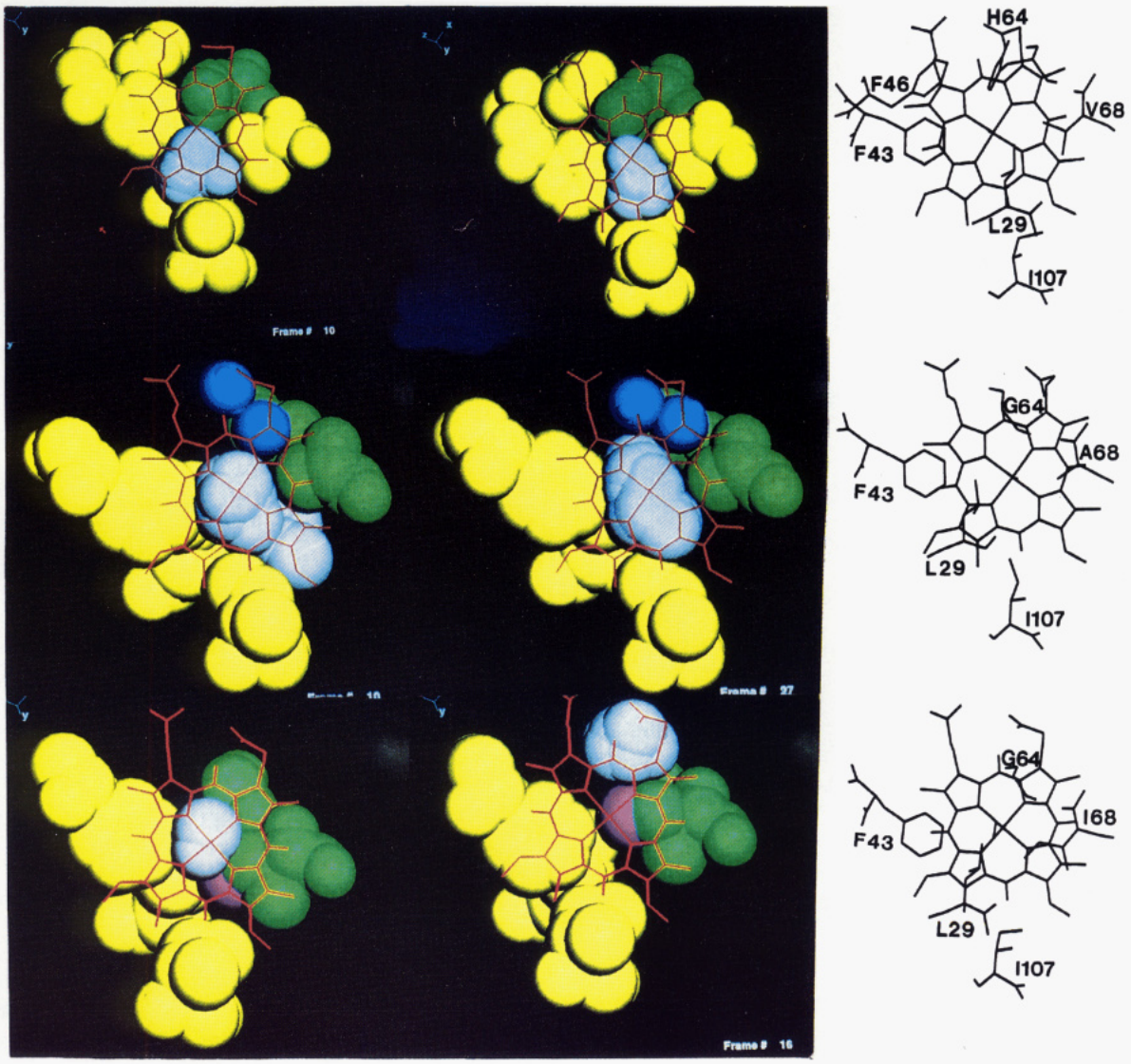

FIGURE 9: Space-filling models of distal residues close to the heme group. The heme group itself is shown as a stick model, and the view is through the heme from the proximal side, in each case. The upper row shows native myoglobin in a simulation run in which the distal histidine (green), at first over the iron atom (left frame), moved away from it. As it did so, the ligand group (white) approached the iron. The middle row shows the double mutant myoglobin G64A68 at two stages in a simulation run, early (left) and later (center) in the run. The mutated residues are in green and the ligands in white. In the early frame, it appears as if ligands are about to pass between Ala68 and Ile107 (left), but they return and continue in line with the iron atom (center). Note the water molecules (blue) which replace the distal histidine. The lower row shows the double mutant G64I68. Again the mutated residues are in green, except for C_δ of Ile68, which is in purple. The left figure shows the ligands beyond the iron, early in the simulation run. The center figure shows that later in the run the ligands have moved away from the iron and their place has been taken by C_δ of Ile68, blocking return of ligands to the iron. Water molecules (not shown) intersect the top of the panel and prevent ligand escape.

(eight) were sufficient (Gibson et al., 1992). Detailed studies of the distribution of water molecules around native myoglobin have recently appeared and are very relevant to the simulation results (Lounnas & Pettitt, 1992; Lounnas et al., 1994).

The effect of steric hindrance on ligand recombination is critically dependent on the location of the ligand group relative to the iron atom, and this, in turn, depends on the positions of the side chains of the heme pocket residues and the initial velocities of their atoms. This is particularly clear for native myoglobin where the average distances from the iron in the two examples of Figure 5 differ by only 1 Å. The large variance in the number of collisions in response to change in the distribution of initial velocities in the simulations (Figure 3) may occur because of differences in the position of the side chain of His64 (Gibson et al., 1992). It may be concluded, therefore, that a single protein trajectory for native myoglobin is not self-averaging in a time of tens of picoseconds.

There is less effect of varying the initial distribution of velocities in the two mutants than in native myoglobin, perhaps for different reasons. In G64I68 the ligand group is located at one edge of the heme after C_δ of 68Ile has moved toward the iron (Figure 9), and the movements of the side chains may simply not be large enough to allow the ligands to approach the iron and increase the collision count. In G64A68, the movement of ligands in a larger space, which usually includes the iron atom, makes the collision count less dependent on the precise position of the side chains. In other words, the rapid exchange between alternate protein coordinates, possible when a larger transient volume is available, makes the individual trajectories more similar, on the average.

All the discussion so far has been predicated on the assumption that ligand rebinding depends solely on the exact positions of the side chains in the distal heme pocket. It has recently been suggested that the nonexponential behavior in NO rebinding (Figure 2) derives from movement of the iron atom out of the heme plane toward the proximal histidine. This movement may well be associated with changes in heme reactivity, but three considerations suggest that it is unlikely

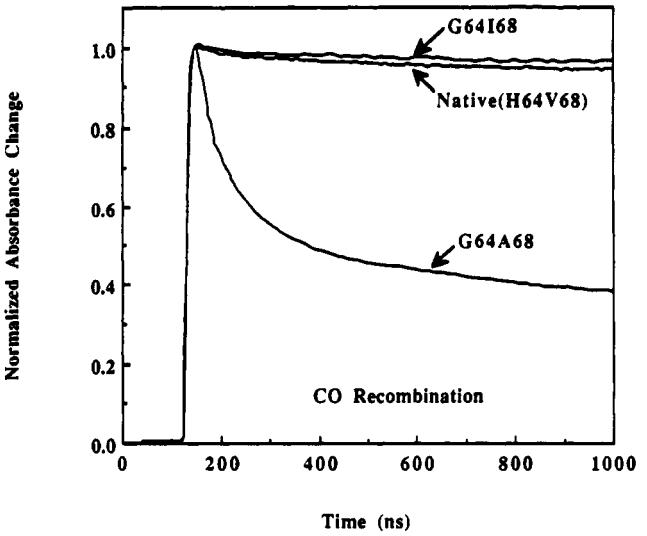

FIGURE 10: Time courses for geminate rebinding of CO to native, G64A68, and G64I68 myoglobins. The conditions were the same as those for Figure 2, except that a 9-ns photolysis pulse was used [see Gibson et al. (1992)].

to account for the behavior of the mutants reported in Figure 2. First, several independent computations have agreed in finding that the movement of the iron is substantially complete in the first picosecond after breaking of the ligand bond (Henry et al., 1985; Petrich et al., 1991; Li et al., 1993). Such a time scale is far too short to be reflected in ligand recombination which, even for NO, requires a half-time of the order of 10 ps or more. Second, experiments with myoglobin in which heme was replaced by cobalt porphyrin have yielded results closely similar to those with heme. Although there is no X-ray evidence about the position of cobalt in myoglobin itself, X-ray results for substituted hemoglobin have shown that cobalt does not move significantly out of the porphyrin plane (Hoard & Scheidt, 1973; Fermi et al., 1982). The contribution made by the motion of the iron is, therefore, not yet clear. Third, if iron relaxation is the cause of nonexponential kinetics, it is to be expected that mutations on the distal side, while affecting amplitude and quantum yield, will not have a qualitative effect on the time course of ligand recombination. The G64A68 mutant, however, comes close to showing single-exponential kinetics. The fluctuating volume and transitions between protein conformations on the distal side suggest a simple explanation. In the double mutant G64A68, two side chains were replaced by smaller ones. The transient volume was increased, and a rapid exchange between the relevant protein conformations became possible. This is also reflected in the smaller variance in the number of collisions between trajectories. Therefore, the limit of rapid exchange is approached, leading toward single-exponential behavior. Such an explanation is also consistent with the data for the computed structural movement shown in Figure 8 where G64A68 is obviously more mobile than either G64I68 or native myoglobin.

The rapid rates of NO recombination observed both experimentally and theoretically for G64A68 myoglobin demonstrate that the innermost barrier to ligand binding is markedly reduced when the sizes of residues 64 and 68 are decreased. This result explains the abnormally high overall rate constant for CO association ($\sim 5 \times 10^7$ $M^{-1}s^{-1}$) which has been reported for this mutant (Egeberg et al., 1990). In native myoglobin, CO binding is limited by a very slow rate of bond formation at the iron atom. This restriction is removed in the G64A68 double mutant, resulting in a 100-fold increase in the overall rate of CO binding. Only 10-fold increases in the bimolecular rate constants for O_2 and NO binding are observed for the G64A68 double mutant since the binding of these ligands to native myoglobin is limited partly or completely by outer kinetic barriers involving ligand motion into and out of the protein (Egeberg et al., 1990; Carver et al., 1990).

In contrast to the results for G64A68 myoglobin, the overall rate of CO binding to the G64I68 double mutant is 2-fold smaller than that for the native protein (Egeberg et al., 1990). This result is consistent with the geminate recombination time courses shown in Figures 2 and 10. The isoleucine side chain at position 68 sterically restricts access to the iron atom and raises the innermost kinetic barrier markedly, even when His64 (E7) has been replaced with Gly.

The success of the molecular dynamics simulations came as a pleasant surprise to the authors of the work described here and in a previous paper (Gibson et al., 1992). Molecular dynamics has correctly reproduced and explained the geminate recombination of nitric oxide with a series of mutants. The approximate LES methodology reproduced the order of recombination rates in the different mutants correctly without adjustment of the parameters of the molecular dynamics code already available (Elber et al., 1994). This direct comparison between experiment and theory on the kinetics of a biomolecule increases confidence in the predictive capabilities of this type of calculation. Furthermore, additional theoretical tests using more elaborate models (Li et al., 1993; Ulitsky & Elber, 1994) have agreed quite well with the qualitative predictions of LES. The higher efficiency of computing with LES suggests the use of this computational method as a tool for the design of other mutants and for better understanding of existing experimental results.

ACKNOWLEDGMENT

We thank Robert Arduini and Mike Quillin for help with structure determination of the double mutant and Eileen Singleton for preparing the protein samples.

REFERENCES

Agmon, N., & Rabinovich, S. (1992) *J. Chem. Phys. 97*, 7270–7286.

Ansari, A., DiIorio, E. E., Dlott, D. D., Frauenfelder, H., Iber, I. E. T., Langer, P., Roder, H., Sauke, T. B., & Shyamsunder, E. (1986) *Biochemistry 25*, 3139–4001.

Austin, R. H., Beeson, K. W., Eisenstein, L., Frauenfelder, H., & Gunsalus, I. C. (1975) *Biochemistry 14*, 5355–5373.

Brunger, A. T., & Karplus, M. (1988) *Proteins 4*, 148–156.

Carver, T. E., Rohlfs, R. J., Olson, J. S., Gibson, Q. H., Blackmore, R. S., Springer, B. A., & Sligar, S. G. (1990) *J. Biol. Chem. 265*, 20007–20020.

Carver, T. E., Brantley, R. E., Jr., Singleton, E. W., Arduini, R. M., Quillin, M. L., Phillips, G. N., Jr., & Olson, J. S. (1992) *J. Biol. Chem. 267*, 14443–14450.

Case, D. A., & Karplus, M. (1979) *J. Mol. Biol. 132*, 343–368.

Cornelius, P. A., Steele, A. W., Chernoff, D. A., & Hochstrasser, R. M. (1981) *Proc. Natl. Acad. Sci. U.S.A. 78*, 7526–7529.

Egeberg, K. D., Springer, B. A., Sligar, S. G., Carver, T. E., Rohlfs, R. J., & Olson, J. S. (1990) *J. Biol. Chem. 265*, 11788–11795.

Elber, R., Roitberg, A., Simmerling, C., Goldstein, R. F., Verkhivker, G., Li, H., & Ulitsky, A. (1994) MOIL: A molecular dynamics program with emphasis on conformational searches and reaction path calculations, in *Statistical mechanics, protein structure and protein substrate interactions* (Doniach, S., Ed.) Plenum Press New York (in press).

Fermi, G., Perutz, M. F., Dickinson, L. C., & Chien, J. C. W. (1982) *J. Mol. Biol. 155*, 495–505.

Gibson, Q. H., Regan, R., Elber, R., Olson, J. S., & Carver, T. E. (1992) *J. Biol. Chem. 267*, 22022–22034.

Hoard, J. L., & Scheidt, W. R. (1973) *Proc. Natl. Acad. Sci. U.S.A. 70*, 3919–3922.
Ikeda-Saito, M., Dou, Y., Yonetani, T., Olson, J. S., Li, T., Regan, R., & Gibson, Q. H. (1993) *J. Biol. Chem. 268*, 6855–6857.
Johnson, K. A., Olson, J. S., & Phillips, G. N., Jr. (1989) *J. Mol. Biol. 207*, 459–463.
Jongeward, K. A., Marsters, J. C., Mitchell, M. J., Magde, D., & Sharma, V. S. (1986) *Biochem. Biophys. Res. Commun. 140*, 962–966.
Jongeward, K. A., Magde, D., Taube, D. J., Masters, J. C., Traylor, T. G., & Sharma, V. S. (1988) *J. Am. Chem. Soc. 110*, 380–387.
Jorgensen, W. L., Chandrasekhar, J., & Madura, J. D. (1983) *J. Chem. Phys. 79*, 7270–7286.
Kabsch, W. (1988) *J. Appl. Crystallogr. 21*, 916–924
Kottalam, J., & Case, D. A. (1988) *J. Am. Chem. Soc. 110*, 7690–7697.
Li, H., Elber, R., & Straub, J. E. (1993) *J. Biol. Chem. 268*, 17908–17916.
Lounnas, V., & Pettitt, B. M. (1992) *J. Phys. Chem. 96*, 7157–7159.
Lounnas, V., Pettitt, B. M., & Phillips, G. N., Jr. (1994) *Biophys. J. 66*, 601–614
Olson, J. S., Mathews, A. J., Rohlfs, R. J., Springer, B. A., Egeberg, K. D., Sligar, S.G., Tame, J., Renaud, J. P., & Nagai, K. (1988) *Nature 335*, 265–266.
Petrich, J. W., Poyart, C., & Martin, J. L. (1988) *Biochemistry 27*, 4049–4060.
Petrich, J. W., Lambry, J. C., Kuczera, K., Karplus, M., Poyart, C., & Martin, J. L. (1991) *Biochemistry 30*, 3975–3987.
Phillips, G. N., Jr., Arduini, R. M., Springer, B. A., & Sligar, S. G. (1990) *Proteins 7*, 358–365.
Quillin, M. L., Arduini, R. M., Olson, J. S., & Phillips, G. N., Jr. (1993) *J. Mol. Biol. 234*, 140–155.
Richard, L., Genberg, L., Deak, J., Chiu, H., & Miller, R. J. D. (1992) *Biochemistry 31*, 10703–10715.
Roitberg, A., & Elber, R. (1991) *J. Chem. Phys. 95*, 9277–9287.
Ryckaert, J. P., Ciccotti, G., & Berendsen, H. J. C. (1977) *J. Comput. Phys. 23*, 327–341.
Smerdon, S. J., Dodson, G. G., Wilkinson, A. J., Gibson, Q. H., Blackmore, R. S., Carver, T. E., & Olson, J. S. (1991) *Biochemistry 30*, 6252–6260.
Springer, B. A., & Sligar, S. G. (1987) *Proc. Natl. Acad. Sci. U.S.A. 84*, 8961–8965.
Ulitsky, A., & Elber, R. (1994) *J. Phys. Chem. 98*, 1034–1043.
Walda, K. N., Liu, X. Y., Sharma, V. S., & Magde, D. (1994) *Biochemistry 33*, 2198–2209.